System integration and coupled effects of an OWT/WEC device

Chenyu Zhao [a], Philipp R. Thies[a], Qi Ye [b], Johanning Lars [a,c]

[a] Renewable Energy Group, College of Engineering, Mathematics and Physical Sciences, University of Exeter

[b] COAST Engineering Research Group, School of Engineering, Faculty of Science and Engineering, University of Plymouth

[c] Naval Architecture, Harbin Engineering University, Nantong Main Street 145, Nangang District, Harbin, China;

Abstract

This paper uses a fully nonlinear model to comprehensively explore the coupled effects caused by the system integration between an offshore wind turbine and a heaving buoy wave energy converter. Parameters of the study include the pitch motion of wind turbine, the tension on the mooring line, the contact pressure between these two devices, and the energy absorbed by power take-off (PTO) system. Results demonstrated that the buoy stabilises/reduces the pitch motion of wind turbine when its metacentric height is positive. A buoy with a negative metacentric height will increase the pitch amplitude of wind turbine and the tension of the mooring line, which is undesirable. The relative vertical motion between heaving buoy and spar could buffer their maximum contact pressure. The Coulomb PTO could offer a higher peak output power of WEC than the linear PTO. The relationship between contact pressure and WEC peak power is quantified to inform the PTO design. The wind/wave device is evaluated at a representative site with suitable wind and wave conditions off the US West Coast. The WEC does significantly reduce the wind turbine pitch motion by at least 60%/50% for the modelled average/max wave conditions with increased power production (14%/80%).

Keywords: Offshore wind turbines, Wave energy converters, Coupled effects, System integration, Power take-off

List of key symbols

m	Mass of heaving buoy
F_r	Wave radiation force
F_e	Wave exciting force
F_{PTO}	PTO force
F_j	The total first-order hydrodynamic force on j-th
F_c	Contact force between the spar and the heaving buoy
c	Hydrostatic stiffness coefficient
φ_1	First order incident wave potential with unit wave amplitude
φ_e	Exciting wave potential
φ_{rj}	Radiation wave potential
φ_d	Diffraction potential
$\varphi_{\triangle dspar}\left(\vec{X}\right)$	Additional diffraction potential
$\varphi_{\triangle sparkr}\left(\vec{X}\right)$	Additional radiation potential
C_{Di}	Drag coefficient of the spar under the i degree of freedom
C_{Mi}	Added mass coefficients of the spar under the i degree of freedom
D_{spar}	Diameter of the spar
u_i	Velocity of the spar under the i degree of freedom
K_u	Spring coefficient
Δl	Deformation of the mooring line
α	Incidence angle
ρ_{air}	Air density
A_{blade}	Element area
c_{blade}	Chord of the blade
$C_{L-blade}(\alpha), C_{D-blade}(\alpha),$ $C_{M-blade}(\alpha)$	Lift, drag and moment coefficients on the α
F_{PTO}	PTO force
C_{PTO}	PTO damping coefficient
$\dot{z}(t)$	The relative velocity along the spar between the heaving buoy and the spar
H	Wave height
T	Wave period
λ	Wavelength
R	Radius of the heaving buoy
R_1	Ratio between wavelength and heaving buoy radius
R_0	The height to radius ratio of heaving buoy

R_2	Pitch ratio with/without the heaving buoy
R_3	Tension ratio with/without the heaving buoy
F_c	Contact force between the heaving buoy and spar
S_c	Contact area between the heaving buoy and the spar

1. Introduction

Traditional energy conversion methods based on fossil fuels represent more than 80% of the world's energy supply. In 2015, a deal was agreed at the United Nations Climate Change Conference in Paris to limit the global rise in temperature over the 21st century to less than two degrees above pre-industrial levels. This increase will require reducing fossil fuel utilisation and, as a result, there is an increasing need for safe, clean, and cheap renewable energy (Dudley, 2018; Robbins, 2016). Wind energy provided the most significant contribution (1.4 EJ) to renewable growth owing to its high energy density and worldwide distribution, and it could be captured and converted by the wind turbine(Gualtieri, 2019). Generally, wind turbines could be classified into onshore and offshore types in accordance with the working location (Porté-Agel et al., 2020; Wu et al., 2019). Compared to onshore devices, offshore wind turbine (OWT) has a relatively higher-capacity power and a more flexible deployment (Arrambide et al., 2019; Wang et al., 2018).

Recently, OWTs have made considerable research and industrial progress. Wang et al. (2018) gave a very comprehensive review of the OWT developments. It could be determined that these developments have already provided great opportunities for wave energy converters (WEC). For an OWT/WEC system, WEC could supply extra output power to reduce the Levelized Cost of energy (Haji et al., 2018; Karimirad and Koushan, 2016). However, the stability and hydrodynamic response of OWT would be influenced (Zhou et al., 2020). The contact force between WEC and OWT is another risk for the structural of the whole system. Focusing on these challenges, researchers have tried to seek possible solutions and obtained significant progress in the system integration of WEC and OWT. Muliawan et al. (2013) investigated the structural responses of a WEC/OWT system, including a spar-type wind turbine and a point absorber WEC via a survival model. In this study, the WEC is believed to reduce the pitch motion of the OWT while the tension force of the mooring line and the bending moment on the OWT

spar would be increased under extreme conditions. In another study concerning the device survival (Wan et al., 2015), the WEC buoy was fixed two different positions on the OWT spar (at the mean water surface and fully submerged). The results determined that when the buoy was fixed under the water surface, motions of the wind turbine could be significantly reduced. (Cheng et al. (2019) proposed a combined concept with a spar-type floating vertical axis OWT and a point absorber WEC and explored their coupled effects under irregular waves and turbulent winds. In this case, the WEC does not change the capture performance of OWT, while it could increase the OWT's heave motion. In (Li et al., 2018b), a tidal current device was integrated into an OWT/WEC system. Its results showed that the whole system had a more significant output power with a smaller pitch and surge motion caused by the system integration. However, the mooring tension was increased by the tidal device and WEC. Similar results are reported in a recent study (Hu et al., 2020), too. The integrated WEC not only increased the total power of the OWT/WEC but also reduced the pitch motion of the OWT. In the summarised literature, most of the added WECs belong to the class of point absorber systems because its capture performance is independent of the incident wave direction (Drew et al., 2009). The coupled effects caused by other types of WECs are also discussed in some studies (Ren et al., 2020; Shi et al., 2018). In (Michailides et al., 2016), the mooring tension, the nacelle acceleration and the bending moment in the OWT's base were not increased with a flap-type WEC.

Some other researchers focused on the effects caused by the power take-off system (PTO) of WEC. Karimirad and Koushan (2016) found that some coupled effects caused by WEC could be minimised with a suitable PTO damping. Wan et al. (2016) used the different damping levels of PTO to investigate the motions of the spar torus combination and mooring line forces. Different PTO damping did not affect horizontal motions of spar such as surge, pitch and mooring line forces. However, this result was only suitable for the WEC with a particular demission with a linear PTO. For a system housing an OWT with three Oscillating Water Columns WECs, PTO damping could change the natural periods of heave, roll and pitch of the whole system (Sarmiento et al., 2019). Borg et al. (2013) determined the PTO damping, which could lead to maximum energy extraction from the WEC or maximum motion reduction of the OWT in an OWT/WEC system. However, these effects caused by PTO would be very small as OWT platforms are much larger compared to the WEC dimension (Lee et al., 2018).

The presented literature explores individual WEC dimensions and only one type of PTO system. Thus, some of the results might lack general applicability. This paper used a fully nonlinear model to comprehensively explore the coupled effects caused by the system integration between an OWT and a heaving buoy WEC. Three buoys with different dimensions matching with both linear and nonlinear PTO are used to obtain a broader scope. The application of real sea states for a potentially suitable suite gives the results a high degree of applicability. The remainder of this paper is organised as follows: Section 2 introduced the concept of the OWT/WEC system used in this paper. Section 3 presented the analytical model. Section 4 exhibits the numerical model as well as its results and discussions, whereas section 5 presents the motion response and power capture for a coupled system off the US West coast. The main findings and conclusions are drawn in Section 6.

2. Conceptual design

This device coupled an OWT and a heaving buoy WEC (Figure 1). The wind turbine is known as the NREL-5MW, housing the generator gearbox hub, blades and a blade control system. The characteristics of the NREL-5MW wind turbine are publicly available and is very widely used as a reference turbine throughout the research community (Pillai et al., 2018). The capacity power of the generator is 5MW. To meet the requirement of the generator rotation speed, the ratio of the gearbox is 97. Each blade is 61.5m, and the blade nodes are directed along the blade pitch axis from the blade root. The control method of the blade and the spar details are presented in a study of OC3 Hywind (Jonkman et al., 2009), which provides the functionality to model variable rotor speed and variable blade-pitch throughout the dynamic simulation. The heaving buoy WEC is also illustrated in Figure 1. The PTO equipped in the WEC is based on a hydraulic system which could supply linear and Coulomb damping (António, 2008; Gaspar et al., 2016). The wind turbine is anchored to the seabed with three mooring lines, shown in Figure 2. Three anchors are deployed around the spar, with an 854m anchor radius to the centre of the spar and 120^{o} azimuth increments. (Figure 2). The primary purpose of this study is to discuss the coupled effects caused by the WEC. The work focussed on modelling deep-water conditions, as this will be the primary

location for floating wind installations. As a result, the (finite) water depth effects are not considered in this study

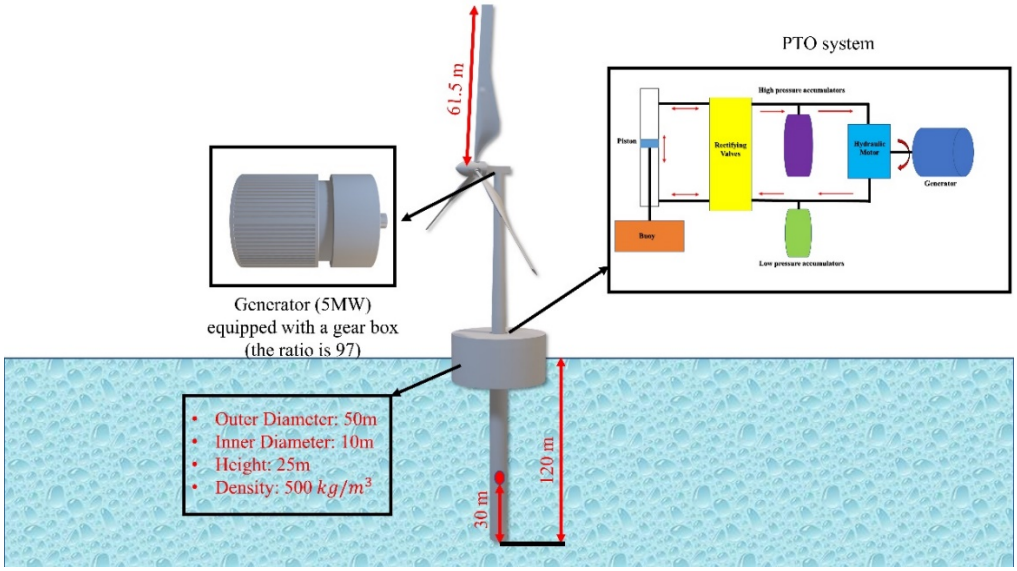

Figure 1: The coupled concept of the floating wind turbine and the heaving buoy WEC

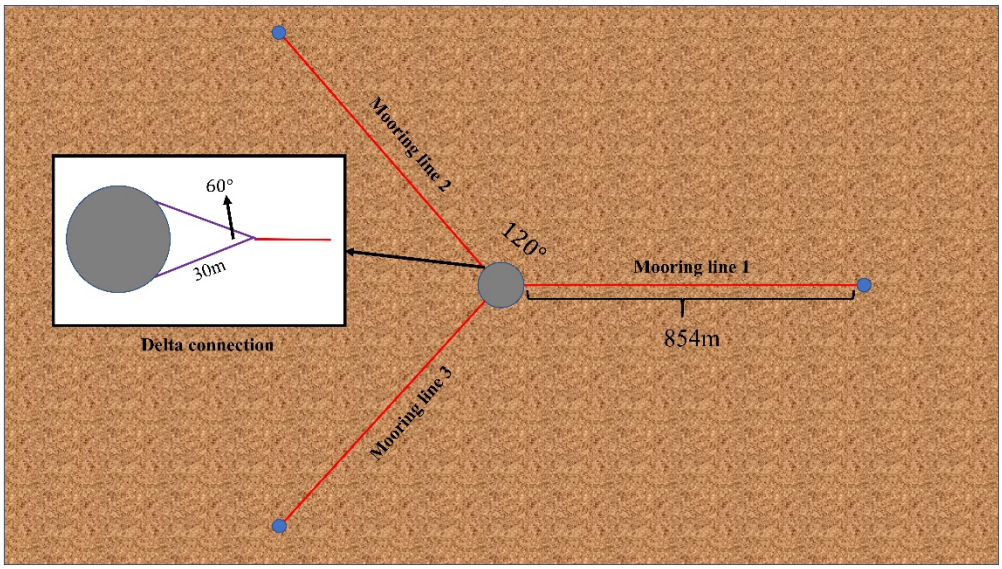

Figure 2: The layout of the mooring system: The length of the main mooring line is 854m, the delta mooring line is 30m, water depth is 320 m.

3. Analytical modelling

3.1 Wave load

The wave force is calculated based on the potential flow theory. For the heaving buoy, the wave load is the sum of exciting force (including diffraction and Froude-Krylov

forces) and radiation force (Figure 3). The response of the buoy is described by solving the following equation:

$$m\ddot{x} = F_r + F_e + F_{PTO} + F_c + cx \tag{1}$$

where m is the mass of heaving buoy, F_r is radiation force, F_e is exciting force, F_{PTO} is PTO force, and F_c is contact force between the spar and the heaving buoy. The variable c is hydrostatic stiffness coefficient owing to the buoyancy and is constant here for sufficiently small deflections.

Due to the incident, radiation and diffraction wave, the isolated space term $\varphi(\vec{x})$ with a particular case of unit amplitude $A = 1$ m in finite water depth can be presented as:

$$\varphi(\vec{x})e^{-i\omega t} = \left\{(\varphi_1 + \varphi_e) + \sum_{6}^{j=1}\varphi_{rj}x_j\right\}e^{-i\omega t} \tag{2}$$

where φ_1 is the first order incident wave potential with unit wave amplitude, φ_e is the corresponding exciting wave potential, φ_{rj} is the radiation wave potential due to the $\mathrm{j}-th$ motion with unit motion amplitude.

The total first-order hydrodynamic force on j-th can be written as:

$$F_j = [(F_{Ij} + F_{dj}) + \sum_{k=1}^{6} F_{rjk}] \tag{3}$$

The spar does not change the incident wave potential of the buoy while it could influence the buoy's radiation and diffraction potentials. As a result, the F_{Ij} is the $j-th$ Froude-Krylov force due to incident wave is written as:

$$F_{Ij} = -i\omega\rho \int_{S_{wet}} \varphi_I(\vec{X}) n_j dS \tag{4}$$

the $j-th$ diffraction force due to diffraction wave is:

$$F_{dj} = -i\omega\rho \int_{S_{wet}} [\varphi_d(\vec{X}) + \varphi_{\triangle dspar}(\vec{X})] n_j dS \tag{5}$$

where the $\varphi_{\triangle dspar}(\vec{X})$ is the additional diffraction potential caused by the spar.

The $j-$th radiation force induced by the $k-$th unit amplitude motion is:

$$F_{rjk} = -i\omega\rho \int_{S_{wet}} [\varphi_{rk}(\vec{X}) + \varphi_{\triangle sparkr}(\vec{X})] n_j dS \tag{6}$$

where the $\varphi_{\triangle sparkr}(\vec{X})$ is the additional radiation potential caused by the spar.

The radiation potential $\varphi_{rk}(\vec{X}) + \varphi_{\triangle sparkr}(\vec{X})$ is divided into real and imaginary parts that produce added mass and radiation damping.

$$a(\omega) = \frac{\rho}{\omega} \int_{S_{wet}} Im\left[\varphi_{rk}(\vec{X}) + \varphi_{\triangle sparkr}(\vec{X})\right] n_j dS \tag{7}$$

$$b(\omega) = \frac{\rho}{\omega} \int_{S_{wet}} \mathrm{Re}\left[\varphi_{rk}(\vec{X}) + \varphi_{\triangle sparkr}(\vec{X})\right] n_j dS \tag{8}$$

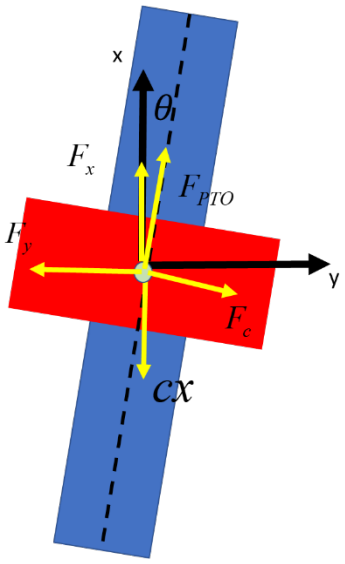

Figure 3:The force diagram of the heaving buoy

For the spar of OWT, owing to its small diameter (comparing to the incident wavelength), its diffraction effect could be ignored, and the wave load is descried by the Morrison equation.

$$F_{spar} = \frac{1}{2} C_{Di} \rho D_{spar} u_i |u_i| + \frac{1}{4} C_{Mi} \rho \pi D^2_{spar} \frac{du_i}{dt} \tag{9}$$

where the C_{Di} and C_{Mi} are the drag and added mass coefficients of the spar under the i degree of freedom, D_{spar} is the diameter of the spar, u_i is the velocity of the spar under the i degree of freedom.

The mooring line of the spar is simplified as a spring, and the tension is presented by:

$$F_{tension} = K_u \Delta l \tag{10}$$

where K_u is the spring coefficient, Δl is the deformation of the mooring line.

3.2 Wind load

The wind load on the blades is calculated individually on each blade mid-segment frame. The loads are due to the inflow ϖ and at incidence angle α, seen in Figure 4(Manual, 2012).

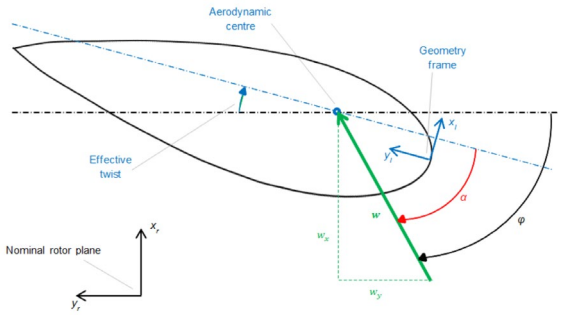

Figure 4: The wind load on the blade of the wind turbine (Manual, 2012)

The lift force in the $w \times z$ direction:

$$f_L = \frac{1}{2} \rho_{air} A_{blade} C_{L-blade}(\alpha) |\omega|^2 \tag{11}$$

The drag force in the w direction:

$$f_D = \frac{1}{2} \rho_{air} A_{blade} C_{D-blade}(\alpha) |\omega|^2 \tag{12}$$

The moment on the pitch:

$$m_z = \frac{1}{2} \rho_{air} A_{blade} c_{blade} C_{M-blade}(\alpha) |\omega|^2 \tag{13}$$

where the ρ_{air} is the air density, A_{blade} is the element area, c_{blade} is the chord of the blade, $C_{L-blade}(\alpha), C_{D-blade}(\alpha), C_{M-blade}(\alpha)$ are the lift, drag and moment coefficients on the α, respectively.

3.3 PTO load

The PTO system provides linear and Coulomb damping forces(Zhao et al., 2020).

The linear PTO force F_{PTO} is proportional to the velocity of the heaving buoy.

$$F_{PTO} = -C_{PTO}\dot{z}(t) \tag{14}$$

where $-C_{PTO}\dot{z}(t)$ is a damping caused by energy extraction, $\dot{z}(t)$ is the relative speed between the heaving buoy and wind turbine along the spar direction,

The Coulomb PTO force is calculated as:

$$F_{PTO} = -sign\left(C_{PTO}, \dot{z}(t)\right) \tag{15}$$

where the direction of the damping force is always opposite to the velocity when the amplitude is a constant value.

4. Numerical modelling

4.1 Model description

An overview of the modelling scope is provided in Figure 5. The numerical simulation in this paper includes a frequency- and a time-domain model. The coefficients of hydrodynamic forces are obtained by the frequency-domain boundary element method solver, namely AQWA (ANSYS, 2013). The physical properties of the spar and WEC configurations are implemented in a coupled nonlinear time-domain model to estimate the hydrodynamic response, the contact pressure and the output power of the heaving buoy experienced by the wind/wave device. The PTO damping is integrated into this model via Python code. The accuracy of the time-domain model with respect to the NREL-5MW OWT has been reported in (Hsu et al., 2015; Sethuraman and Venugopal, 2013; Xu and Srinil, 2015)

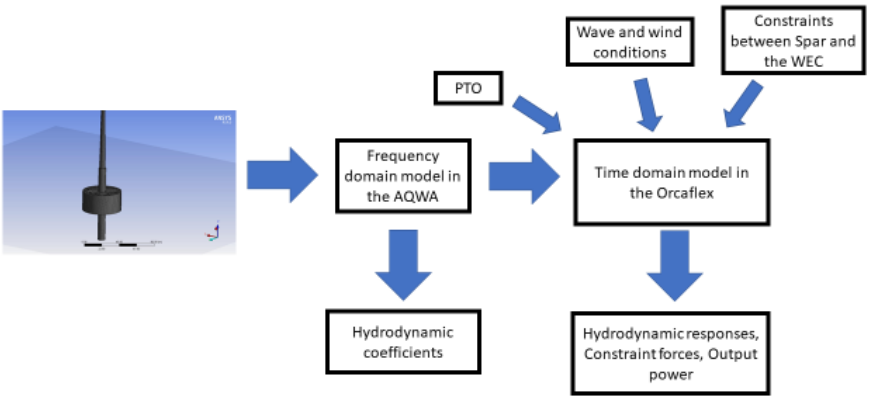

Figure 5: Numerical modelling flowchart

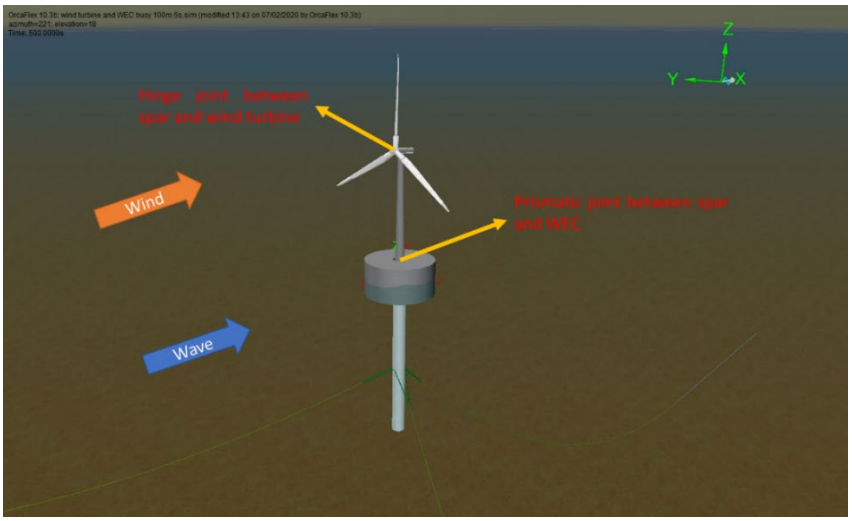

Figure 6: Time-domain model configuration: The incident wave and wind directions are co-linear. Hinge joint and Prismatic joint are used to connect spar with the wind turbine and the WEC, respectively

4.2 Cases

The cases are separated into no-PTO cases and PTO cases. For both, incident waves are regular with a fixed wave height $H = 6$ m and a range of wave periods $T = 6$s to $T = 10$s. The wavelength (λ) of incident waves are normalised by the radius of the heaving buoy (R), presented by $R_1 = \frac{\lambda}{R}$ (ranging from 0.78 to 3.1). The wind load used in all cases is 25 m/s, which is the cut-out speed of the NREL-5MW (Li et al., 2018a). The wind direction is assumed to be collinear with the incident wave direction. During non-PTO cases, three heaving buoys (Figure 7 and) with an identical density (500 kg/m^3) are configured into different height-to-radius ratios (R_0). For PTO cases, only

the buoy with $R_0 = 0.5$ is selected, and this buoy is equipped with both linear and Coulomb damping PTOs. In order to exhibit impacts caused by these heaving buoys and two PTO systems, another two normalised parameters are used as follows:

$R_2 = \frac{A_{buoy}}{A_{nobuoy}}$ where the A_{nobuoy} is the max pitch amplitude of the wind turbine spar without the buoy, the A_{buoy} is the pitch amplitude of the wind turbine spar with the buoy.

$R_3 = \frac{T_{buoy}}{T_{nobuoy}}$ where the T_{nobuoy} is the tension of the mooring line without the buoy, the T_{buoy} is the tension of the mooring line with the buoy.

The contact pressures between the heaving buoy and the spar of the wind turbine is calculated by: $\frac{F_c}{S_c}$, where F_c is the contact force, and the S_c is the contact area.

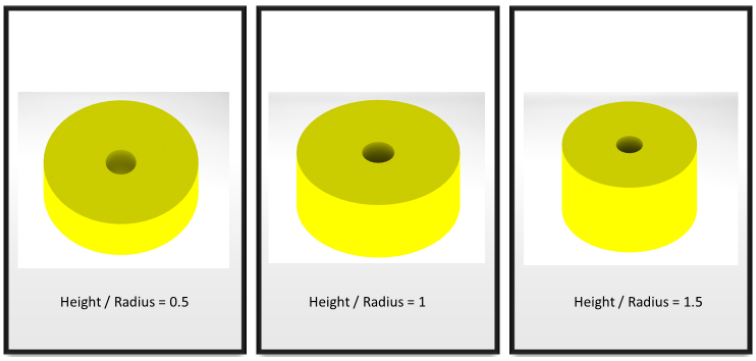

Figure 7: Three buoys with different R_0 used in the non-PTO cases.

Table 1 The properties of three heaving buoys

Properties/Buoy	R_0=0.5	R_0=1	R_0=1.5
Density	500 kg/m^3	500 kg/m^3	500 kg/m^3
Inner Radius	5 m	5 m	5 m
Outer Radius	25 m	25 m	25 m
Height	12.5 m	25 m	37.5 m

4.3 Results

4.3.1 Non-PTO cases

The R_2 parameter of spars, coupled with different heaving buoys, is presented in Figure 8. R_2 shows similar behaviour in all situations and converges towards a value of 1 with growing R_1. Moreover, the buoy with a smaller R_0 could reduce the pitch amplitude of the spar more significantly. Furthermore, when the R_0 is large enough (here, the R_0=1.5), the buoy would increase the motion amplitude of the spar.

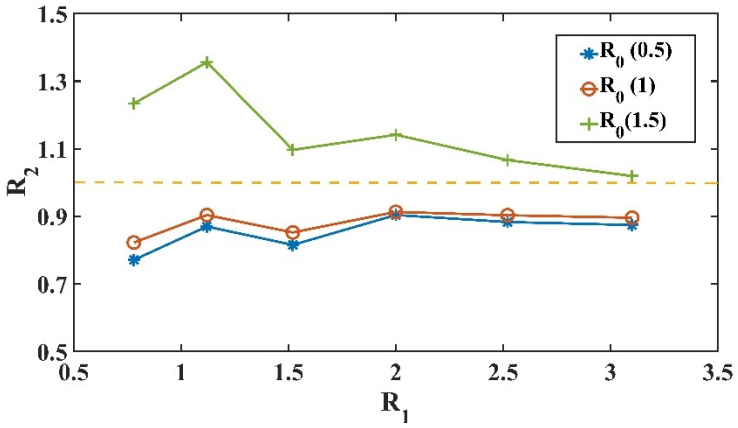

Figure 8: The R_2 of the spar coupled with three different heaving buoys: the area below the dashed line means the max pitch amplitude of the spar will be reduced. The upper area means the pitch amplitude will be increased.

The results R_3 are presented in Figure 9. Owing to line 2 and line 3 are entirely symmetric to the incident wave, the tension is identical on these two mooring lines. It is found that the tension on all mooring lines has increased because of the heaving buoy. Comparing the tension on the line l and the line 2&3, the increased tension amplitude of line 1 is more significant than that of the line 2&3 (here, the maximum amplitudes are 38% and 15%, respectively). Additionally, the buoy with a higher R_0 will lead to a larger tension under the same wave condition, and these tension differences perform more significantly on line 1.

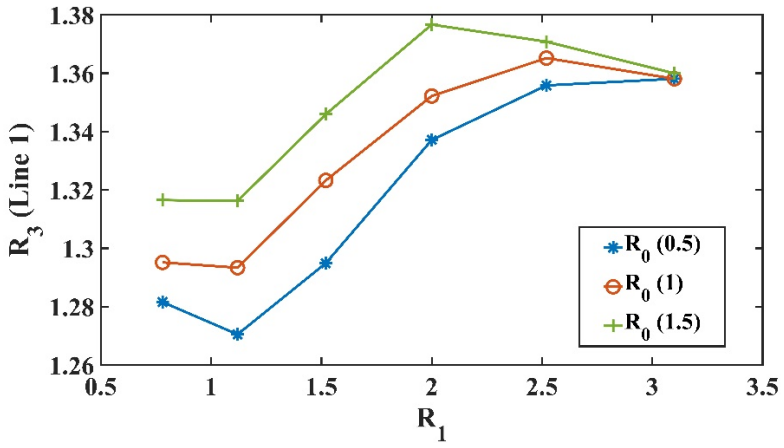

(a)

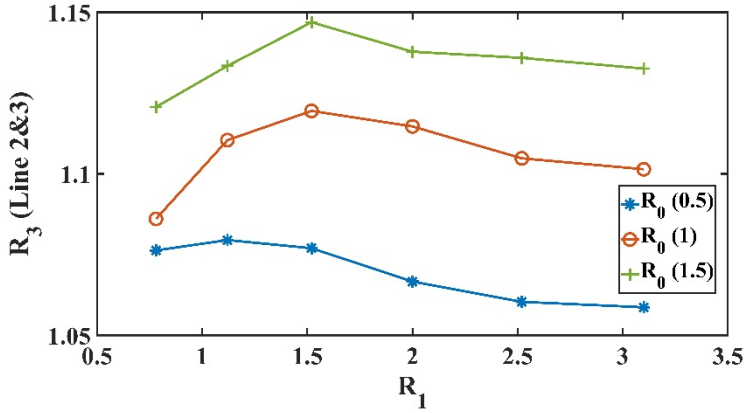

(b)

Figure 9:The tension difference of the mooring lines (a) Line 1; (b) Line 2&3

Figure 10 exhibits the results of the pressure between the spar and the heaving buoy. For all three buoys, the maximum pressure appears at the R_1 =0.78, and the changing rate of the pressure trends to be stable after the R_1 exceeds 2. Comparing the results of three buoys, the buoy with a larger R_0 could offer a smaller pressure between the spar and the heaving buoy.

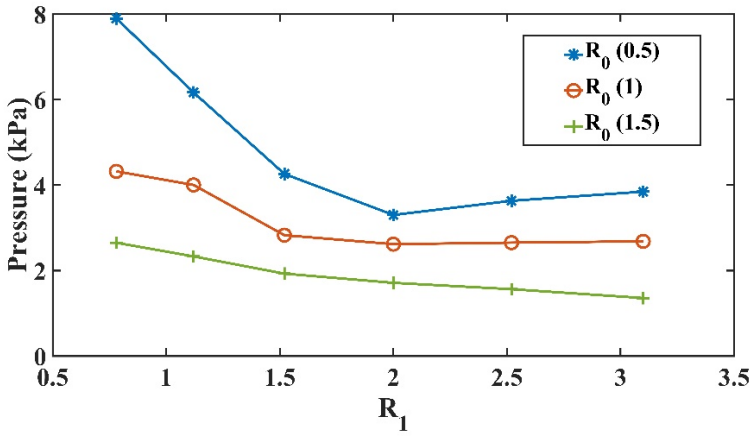

Figure 10: The pressure between the spar and the heaving buoy

4.3.2 PTO cases

In PTO cases, the buoy with R_0=0.5 is selected, and the incident wave is set to be a constant value, R_1=2. Figure 11 presents the average power absorbed by linear and Coulomb PTO with respect to a range of damping values. It can be observed that the average power would increase first to reach a maximum power point before it decreases again with increasing PTO damping. Moreover, the average power absorbed by the Coulomb PTO is more sensitive to damping values. Additionally, the maximum power absorbed by the Coulomb PTO is larger than that by the linear PTO.

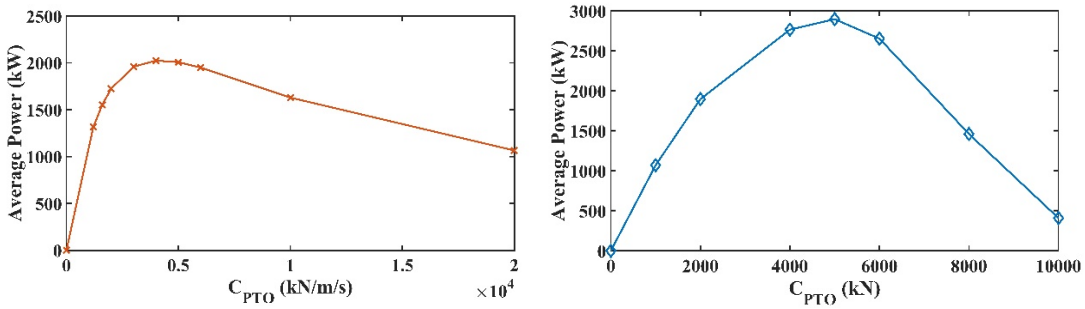

(a) (b)

Figure 11:The average power absorbed by the linear and Coulomb PTO, respectively: (a) Linear PTO; (b) Coulomb PTO

The R_2 of the spar with different damping values are presented in Figure 12. It is found that a larger PTO damping could decrease the pitch motion of the spar and this effect of the Coulomb PTO is much more significant than that of the linear PTO. The result of R_3 follows the same trend as the R_2. The stiffer PTO will decrease the tension of the mooring line (Figure 13).

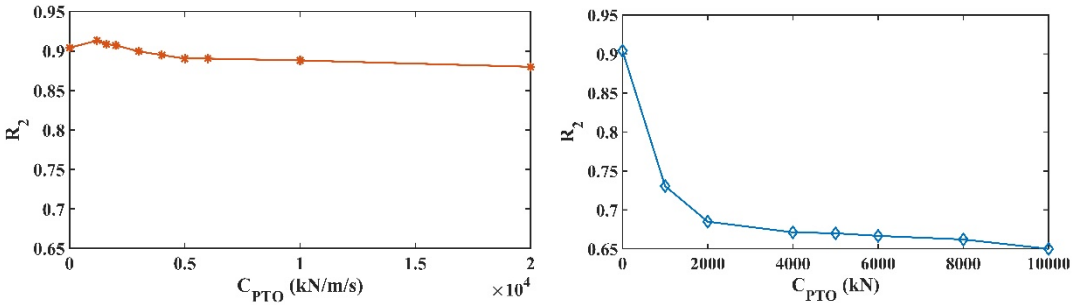

(a) (b)

Figure 12: R_2 of the spar with linear and Coulomb PTO, respectively: (a) Linear PTO; (b) Coulomb PTO

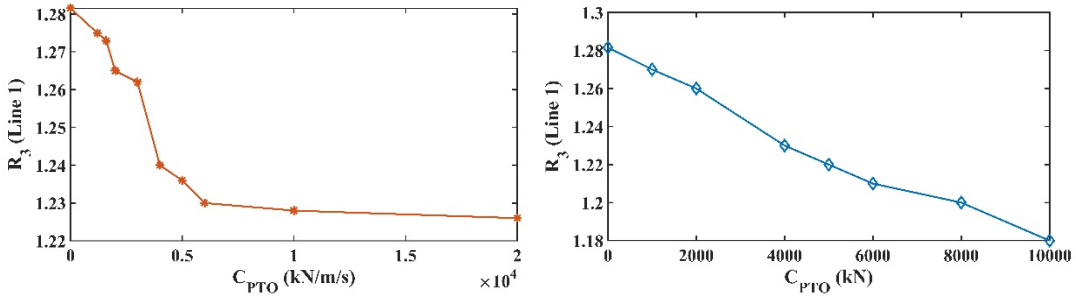

(a) (b)

Figure 13: R_3 of the mooring line 1 with linear and Coulomb PTO, respectively: (a) Linear PTO; (b) Coulomb PTO

For the contact pressure between the heaving buoy and the spar, a larger PTO damping will offer a higher peak value on the contact surface, and the increasing amplitude caused is more evident for the Coulomb PTO (Figure 14).

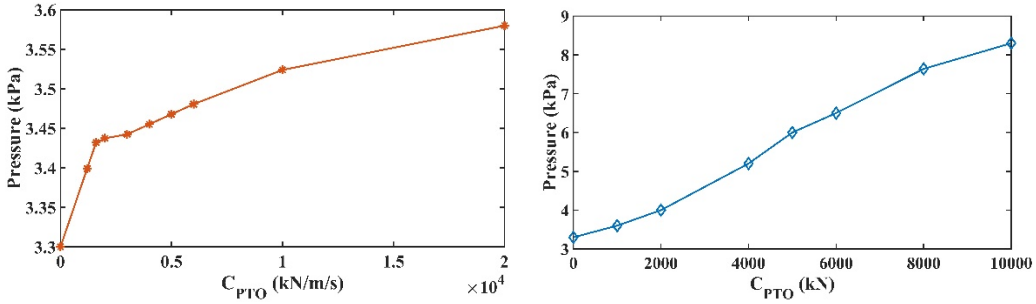

Figure 14:The contact pressure with linear and Coulomb PTO, respectively: (a) Linear PTO; (b) Coulomb PTO

5. Discussions

This paper integrated OWT (NREL-5MW) and a heaving buoy WEC via a fully nonlinear numerical model. The coupled effects were discussed in non-PTO and PTO cases.

5.1.1 Non-PTO cases

Many previous studies have demonstrated that the additional damping offered by heaving buoy could stabilise the motion of OWT. In this situation, the heaving buoy could be considered as a damping plate of the spar, which is a popular design in OWT and WECs. However, when the R_0 of the heaving buoy keeps growing, its stabilisation effects will be weakened. Shown by Figure 8, the stabilisation effect of the heaving buoy is even counterproductive for the spar motion, i.e. increases spar motion when the $R_0 = 1.5$. This destabilising effect is caused by the negative metacentric height of the heaving buoy. When a floating body with the negative metacentric height offsets its balance position, it will produce a large negative restoring torque which cannot be compensated by the additional damping. As a result, the motion amplitude of the wind turbine spar will be activated by this negative restoring moment. Table 2 list metacentric heights and restoring moments of three buoys used in non-PTO cases. Considering the result exhibited in Figure 8, it is found that the buoy with increased positive metacentric height has a more significant stabilisation effect on the wind turbine spar.

Table 2 Metacentric height and restoring moment of the buoy

Buoy	Metacentric height (m)	Restoring Moments ($kN \cdot m/^\circ$)
$R_0 = 0.5$	22.8	4723.9
$R_0 = 1.0$	6.74	2786.4
$R_0 = 1.5$	-0.7	-4509.1

According to the result in Figure 8, the heaving buoy has different stabilisation performance characteristics for a range of incident waves. Owing to the R_2 changing trend is identical for different buoys, the buoy with $R_0 = 0.5$ is selected to discuss the

relationship between the stabilised effect and the incident wave. When R_1 is very large, the period of the incident wave will be extremely long. The value of R_2 will eventually converge towards a value of 1. For incident waves with a relatively smaller R_1, the buoy's stabilising characteristics are relatively weaker compared to the buoy motion amplitude. Figure 10 and Figure 8 show the motion amplitude normalised by the wave height, presented as $R_4 = \frac{motionamplitude}{waveamplitude}$. The buoy seems to have a better stabilising effect for relatively smaller motion amplitudes.

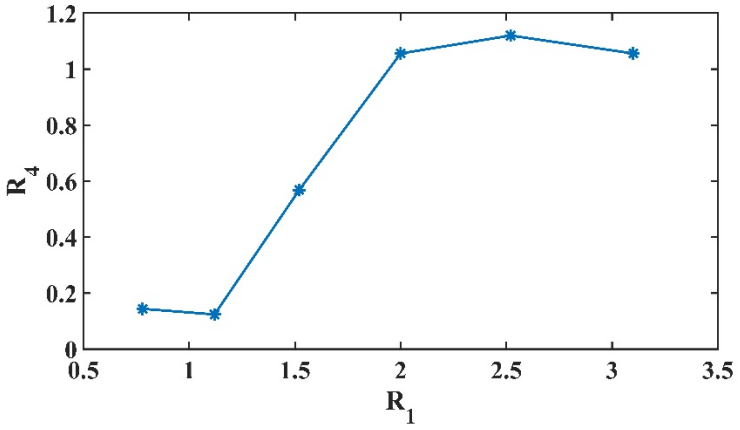

Figure 15: The motion amplitude of the buoy with R_0=0.5 with a range of incident waves

Results in Figure 9 show that the heaving buoy will increase the tension load on the mooring line. This is because the new coupled system with the heaving buoy has a more substantial mass and rotational inertia than the single OWT. Moreover, the increasing amplitude of tension will be more significant for the buoy with a larger mass. For the mooring system in this paper (see Figure 2), line 1 is configured to head the incident wave, which will lead to a larger tension on line 1. Comparing to the result in Figure 15 and Figure 9 (a), the motion amplitude, and the increasing tension of line 1 follow almost the same trend. This means a more vigorous motion of the buoy will significantly increase the tension on line 1(Figure 16).

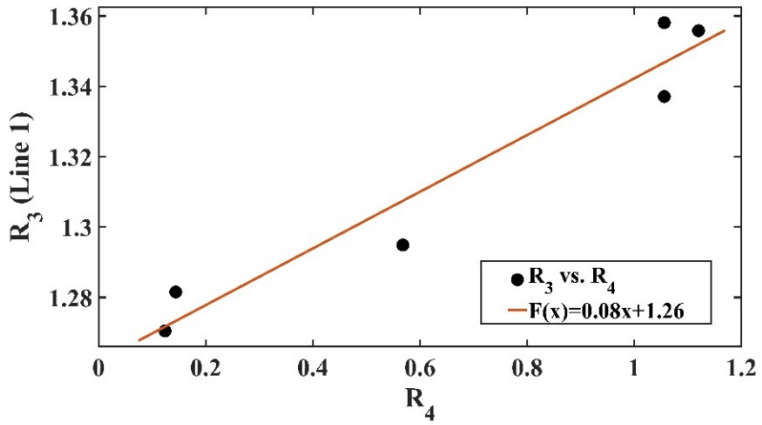

Figure 16: The tension on line 1 with respect to the motion amplitude of the buoy, a corresponding positive relationship

The buoy with a relatively smaller R_0 has a better stabilising effect, while it could produce a larger contact pressure on the surface of the spar because of the narrow contact area, especially under incident waves with short periods. Considering the motion amplitude of the buoy is very tiny under these short-period waves, the connection between the buoy could be regarded as a rigid one which will significantly increase the contact pressure. This contact pressure is buffered by the increasing motion amplitude of the buoy (See Figure 17).

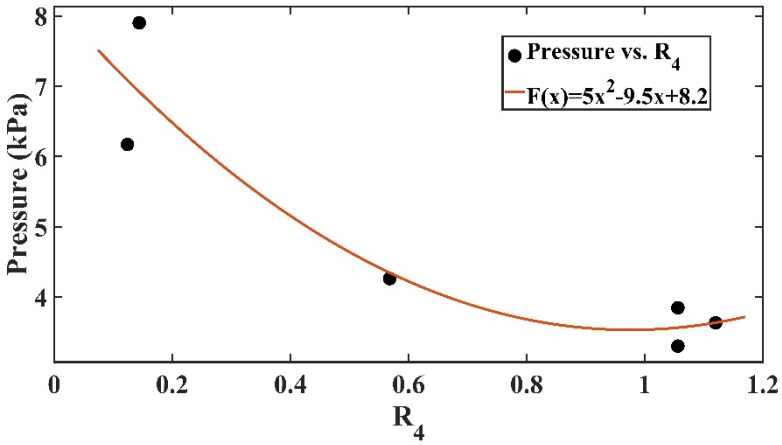

Figure 17: The contact pressure with respect to the motion amplitude of the buoy

5.1.2 PTO-cases

As discussed in section 4.4.1, a more significant motion amplitude of the heaving buoy would bring a larger R_2 and R_3, as well as a smaller contact pressure. Comparing results from the two types of PTO, these effects seem to be more evident in Coulomb

PTO cases, which means the motion of the heaving buoy is more sensitive to the Coulomb damping.

The output power is the critical factor for a WEC, and it could be maintained at a high level via adjusting PTO damping amplitude. As shown in Figure 14, the PTO damping could significantly improve the contact pressure. Figure 18 gives the power of the heaving buoy (Coulomb PTO) with respect to the contact pressure. It is found that the power has a corresponding positive relationship with the contact pressure in the area A (before the power reaches its peak value), which means the maximum output power of the heaving buoy could be designed based on the pressure capacity of the spar surface. For this coupled device, the sustained pressure of the spar should be larger than the 6 kPa if the desired power of the heaving buoy is 3000 kW.

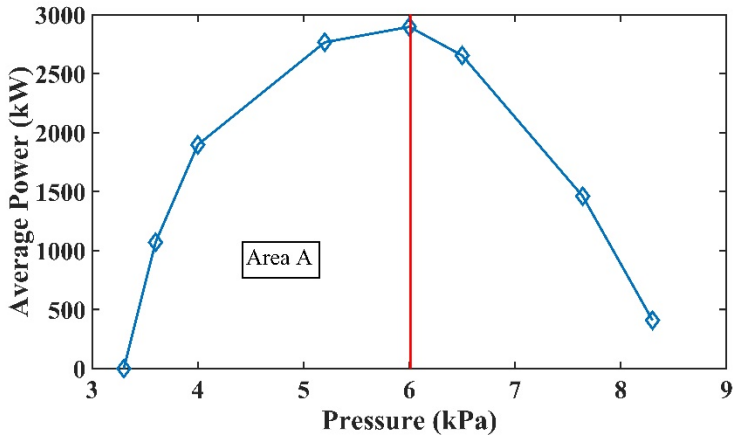

Figure 18: The maximum contact pressure with respect to the power, for the Coulomb PTO

6. Field study

In this section, hydrodynamic and energy capture performances of this OWT/WEC device is assessed under a real sea condition. The potential site with a 345 water depth locates in the west costa of US which theoretical wave energy potential is more than twice that of the East coast (Jacobson et al., 2011), thus making it a potentially suitable site for a coupled Wind/Wave system. Average and extreme wave conditions used in the numeral model are listed in Table 3, according to 10-year wave data recorded by Wave Station 46213 (Figure 19) (Center, 2020). These wave conditions are defined by the JONSWAP spectrum (Figure 20). Based on the results in section 4, the heaving

buoy used here has a 50 m diameter and a 12.5 m height, equipped with a 5,000 kN Coulomb PTO.

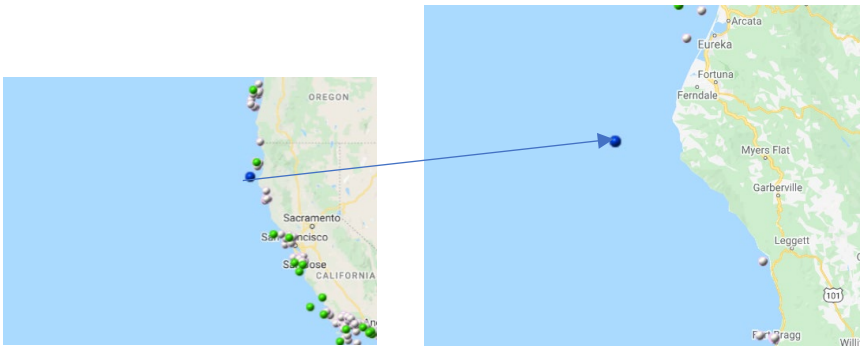

Figure 19: The wave station 46213 in the potential site, 40 17.692' (N), 124 43.906' (W), measured parameters: wave energy, wave direction, sea temperature, water depth = 345 m

Table 3 The input wave condition in the numerical model, based on statistic results of wave station 46213

	Significant wave height (m)	Peak wave period (s)
Average condition	3	12.48
Extreme condition	13	15.38

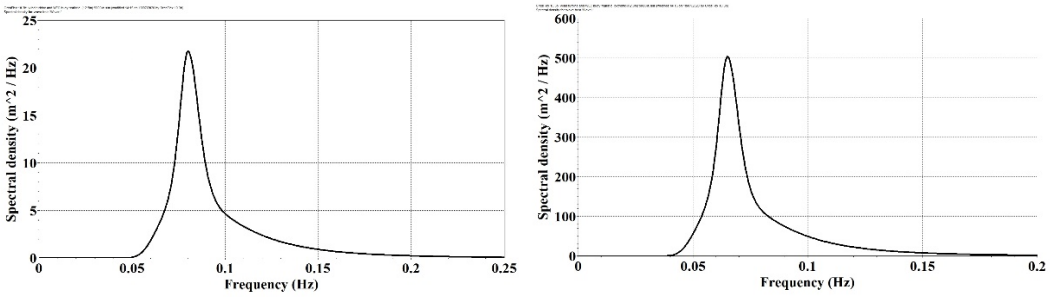

(a) (b)

Figure 20 The wave spectrum used in the case study: (a) Average condition; (b) Extreme condition

Table 4 and Table 5 exhibit the effects caused by the heaving buoy under average and extreme wave conditions. The motion decreased amplitude is slighter larger under the average wave condition. However, the tension increase amplitudes are very similar under both wave conditions.

For power production, the rated power of OWT is considered as its mean power. The heaving buoy WEC could supply a 14% power increase under the average wave condition. The power increase under the extreme wave condition could reach 82%; however, this value might be less meaningful for the realistic environment. The heaving buoy would always be fixed on the spar to protect the PTO system under the extreme condition.

Table 4 Hydrodynamic and capture performance of the combined device under average wave condition

	Pitch reduction	Tension increase	Power increase
Mean	63%	25%	14%
Max	67%	35%	N/A

Table 5 Hydrodynamic and capture performance of the combined device under extreme wave condition

	Pitch reduction	Tension increase	Power increase
Mean	49%	20%	82%
Max	62%	33%	N/A

7. Conclusions

In this paper, a fully nonlinear model was built to integrate an OWT and a heaving buoy WEC. The control method of the wind turbine blades and the hydraulic PTO system of the WEC is included in this model as external Python codes functions. The coupled effects of this OWT/WEC system, housing the pitch motion amplitude of the wind turbine, the tension on the mooring line and the contact pressure between the spar and the heaving buoy, were explored in PTO and non-PTO cases.

In non-PTO cases, this study compared the coupled effects of three buoys with different dimensions. It was found that when the buoy had a positive metacentric height, the pitch motion of the wind turbine is stabilised by the buoy. However, a buoy with a negative metacentric height could increase the pitch motion of the wind turbine, which is undesirable. For all non-PTO cases, the mooring tension increases by up to 40%/30% in regular/irregular waves because of the buoy heaving motion. The results determined

show that a larger motion amplitude could lead to a stronger pitch motion of OWT, a larger tension on the mooring line, as well as a smaller contact pressure on the spar surface.

In PTO cases, linear and Coulomb damping cases are modelled for the PTOs. Compared to the linear PTO, the Coulomb PTO could offer a higher peak power for the WEC system under the same wave condition. The relationship between the contact pressure and the peak power of the heaving buoy has been established. This will allow finding the design contact pressure for WEC in order to maximise power.

The combined OWT/WEC device was numerically tested using real sea conditions of the West coast of the US. Under the average wave condition of the potential site, the heaving buoy could supply a 14% power increase.

The coupled model and the research methods presented in this study provide some new insights into the OWT/WEC system design, motion response and application. However, there are some limitations in the present model, which should be noted here. Firstly, this model relies on the potential flow theory. The additional hydrodynamic damping of the device caused by the liquid viscosity should thus be revised, e.g. through experimental tank tests in the future. Secondly, the heaving buoy WEC did not use any control strategies to improve the power capture. The reported WEC power relates to the power input to the PTO itself. Hydraulic and electrical losses at the generator stage are not considered. The control strategy of the PTO could be further developed and tested as a part of future work.

Acknowledgements

This work has received funding through the EPSRC Supergen ORE Hub [EP/S000747/1]. Qi Ye would like to acknowledge the financial support received from European Commission Research Executive Agency via a Marie Skłodowska-Curie Research and Innovation Staff Exchange project (H2020-MSCA-RISE-2016, RESET-730888).

References

ANSYS, A., 2013. Version 15.0; ANSYS. Inc.: Canonsburg, PA, USA November 752.
António, F.d.O., 2008. Phase control through load control of oscillating-body wave energy converters with hydraulic PTO system. Ocean Engineering 35 (3-4), 358-366.
Arrambide, I., Zubia, I., Madariaga, A., 2019. Critical review of offshore wind turbine energy production and site potential assessment. Electric Power Systems Research 167, 39-47.
Borg, M., Collu, M., Brennan, F.P., 2013. Use of a wave energy converter as a motion suppression device for floating wind turbines. Energy Procedia 35, 223-233.
Center, N.D.B., 2020. National Data Buoy Center.
Cheng, Z., Wen, T.R., Ong, M.C., Wang, K., 2019. Power performance and dynamic responses of a combined floating vertical axis wind turbine and wave energy converter concept. Energy 171, 190-204.
Drew, B., Plummer, A.R., Sahinkaya, M.N., 2009. A review of wave energy converter technology. Sage Publications Sage UK: London, England.
Dudley, B., 2018. BP statistical review of world energy. BP Statistical Review, London, UK, accessed Aug 6, 2018.
Gaspar, J.F., Calvário, M., Kamarlouei, M., Soares, C.G., 2016. Power take-off concept for wave energy converters based on oil-hydraulic transformer units. Renewable Energy 86, 1232-1246.
Gualtieri, G., 2019. A comprehensive review on wind resource extrapolation models applied in wind energy. Renewable and Sustainable Energy Reviews 102, 215-233.
Haji, M.N., Kluger, J.M., Sapsis, T.P., Slocum, A.H., 2018. A symbiotic approach to the design of offshore wind turbines with other energy harvesting systems. Ocean Engineering 169, 673-681.
Hsu, W.-t., Thiagarajan, K.P., MacNicoll, M., Akers, R., 2015. Prediction of extreme tensions in mooring lines of a floating offshore wind turbine in a 100-year storm, International Conference on Offshore Mechanics and Arctic Engineering. American Society of Mechanical Engineers, p. V009T009A050.
Hu, J., Zhou, B., Vogel, C., Liu, P., Willden, R., Sun, K., Zang, J., Geng, J., Jin, P., Cui, L., 2020. Optimal design and performance analysis of a hybrid system combing a floating wind platform and wave energy converters. Applied Energy 269, 114998.
Jacobson, P.T., Hagerman, G., Scott, G., 2011. Mapping and assessment of the United States ocean wave energy resource. Electric Power Research Institute.
Jonkman, J., Butterfield, S., Musial, W., Scott, G., 2009. Definition of a 5-MW reference wind turbine for offshore system development. National Renewable Energy Lab.(NREL), Golden, CO (United States).

Karimirad, M., Koushan, K., 2016. WindWEC: Combining wind and wave energy inspired by hywind and wavestar, 2016 IEEE International Conference on Renewable Energy Research and Applications (ICRERA). IEEE, pp. 96-101.
Lee, H., Poguluri, S.K., Bae, Y.H., 2018. Performance analysis of multiple wave energy converters placed on a floating platform in the frequency domain. Energies 11 (2), 406.
Li, H., Hu, Z., Wang, J., Meng, X., 2018a. Short-term fatigue analysis for tower base of a spar-type wind turbine under stochastic wind-wave loads. International Journal of Naval Architecture and Ocean Engineering 10 (1), 9-20.
Li, L., Gao, Y., Yuan, Z., Day, S., Hu, Z., 2018b. Dynamic response and power production of a floating integrated wind, wave and tidal energy system. Renewable Energy 116, 412-422.
Manual, O., 2012. Online at http://www. orcina. com/SoftwareProducts/OrcaFlex/Documentation. OrcaFlex. pdf.
Michailides, C., Gao, Z., Moan, T., 2016. Experimental study of the functionality of a semisubmersible wind turbine combined with flap-type Wave Energy Converters. Renewable Energy 93, 675-690.
Muliawan, M.J., Karimirad, M., Gao, Z., Moan, T., 2013. Extreme responses of a combined spar-type floating wind turbine and floating wave energy converter (STC) system with survival modes. Ocean Engineering 65, 71-82.
Pillai, A.C., Thies, P.R., Johanning, L., 2018. Mooring system design optimisation using a surrogate assisted multi-objective genetic algorithm. Engineering Optimisation.
Porté-Agel, F., Bastankhah, M., Shamsoddin, S., 2020. Wind-turbine and wind-farm flows: a review. Boundary-Layer Meteorology 174 (1), 1-59.
Ren, N., Ma, Z., Shan, B., Ning, D., Ou, J., 2020. Experimental and numerical study of dynamic responses of a new combined TLP type floating wind turbine and a wave energy converter under operational conditions. Renewable Energy 151, 966-974.
Robbins, A., 2016. How to understand the results of the climate change summit: Conference of Parties21 (COP21) Paris 2015. Springer.
Sarmiento, J., Iturrioz, A., Ayllón, V., Guanche, R., Losada, I., 2019. Experimental modelling of a multi-use floating platform for wave and wind energy harvesting. Ocean Engineering 173, 761-773.
Sethuraman, L., Venugopal, V., 2013. Hydrodynamic response of a stepped-spar floating wind turbine: Numerical modelling and tank testing. Renewable Energy 52, 160-174.
Shi, W., Park, Y., Park, H., Ning, D., 2018. Dynamic analysis of the wind turbine drivetrain considering shaft bending effect. Journal of Mechanical Science and Technology 32 (7), 3065-3072.
Wan, L., Gao, Z., Moan, T., 2015. Experimental and numerical study of hydrodynamic responses of a combined wind and wave energy converter concept in survival modes. Coastal Engineering 104, 151-169.
Wan, L., Gao, Z., Moan, T., Lugni, C., 2016. Experimental and numerical comparisons of hydrodynamic responses for a combined wind and wave energy converter concept under operational conditions. Renewable Energy 93, 87-100.
Wang, X., Zeng, X., Li, J., Yang, X., Wang, H., 2018. A review on recent advancements of substructures for offshore wind turbines. Energy conversion and management 158, 103-119.

Wu, X., Hu, Y., Li, Y., Yang, J., Duan, L., Wang, T., Adcock, T., Jiang, Z., Gao, Z., Lin, Z., 2019. Foundations of offshore wind turbines: A review. Renewable and Sustainable Energy Reviews 104, 379-393.
Xu, X., Srinil, N., 2015. Dynamic response analysis of spar-type floating wind turbines and mooring lines with uncoupled vs coupled models, International Conference on Offshore Mechanics and Arctic Engineering. American Society of Mechanical Engineers, p. V009T009A062.
Zhao, C., Cao, F., Shi, H., 2020. Optimisation of heaving buoy wave energy converter using a combined numerical model. Applied Ocean Research 102, 102208.
Zhou, Y., Ning, D., Shi, W., Johanning, L., Liang, D., 2020. Hydrodynamic investigation on an OWC wave energy converter integrated into an OWT monopile. Coastal Engineering, 103731.